

# Modeling solid-state boron carbide low energy neutron detectors

C. Lundstedt<sup>a,b</sup>, A. Harken<sup>a,c</sup>, E. Day<sup>a,c</sup>, B.W. Robertson<sup>a,c</sup>, S. Adenwalla<sup>a,b,\*</sup>

<sup>a</sup>Center for Materials Research and Analysis, University of Nebraska-Lincoln, Lincoln, NE 68588, USA

<sup>b</sup>Department of Physics and Astronomy, University of Nebraska, Lincoln, Lincoln, NE 68588-0111, USA

<sup>c</sup>Department of Mechanical Engineering, University of Nebraska, Lincoln, Lincoln, NE 68588-0656, USA

Received 16 January 2006; received in revised form 14 February 2006; accepted 15 February 2006

Available online 10 March 2006

## Abstract

Two independent techniques for modeling boron-based solid-state neutron detectors are presented—one using the GEANT4 Monte Carlo toolkit and the other one an analytical approach using a simplified physical model. Results of these techniques are compared for three different types of solid-state boron carbide detector. These results provide the basis for distinguishing between conversion layer and other solid-state detectors.

© 2006 Elsevier B.V. All rights reserved.

PACS: 29.40.Wk

Keywords: Neutron detector; GEANT; Numerical modeling; Semiconductor detector

Neutron detection capabilities have, in general, lagged far behind those for X-rays, primarily due to the absence of an efficient all solid-state neutron detector. The construction of high intensity neutron sources [1], the ever more urgent need for sensitive detection of fissile material and the routine use of neutron detectors on space missions [2–4], would all benefit from the robustness, sensitivity, low mass, small power consumption and size of a true solid-state detector. Present day neutron detectors consist mainly of gas counters (filled with BF<sub>3</sub> [5,6] or <sup>3</sup>He) and scintillators. While research on methods of improving efficiency, optimizing parameters, and reducing the size and cost of these continues, the advent of a working solid-state neutron detector would clearly represent a major advance.

The fundamental limitation on the selection of neutron detector materials is the small neutron capture cross-section of most elements. The list of suitable elements is

small and few lend themselves to the development of a semiconducting solid. Most current solid-state neutron detectors consist of a conversion layer, which captures the neutron, in contact with a semiconducting material or device which detects at most one product of the neutron capture reaction (although sandwich and non-planar conversion layer detectors may allow capture of both products) [7–9]. In an ideal solid state device, the neutron capture material would in fact be an integral part of the device—it would both capture neutrons and produce a signal in response to both products of capture. Such a device would consist of a semiconducting material with a large neutron capture cross-section.

At the University of Nebraska, Lincoln (UNL), a semiconducting form of boron carbide has been developed over the last 15 years [10–12] and made into homojunction diodes, heterojunction diodes and a variety of transistors [13–16]. We have recently demonstrated the viability of using boron carbide (BC)/silicon heterojunction diodes as neutron detectors [17,18]. Although the BC layer was very thin, making its results essentially indistinguishable from conversion layer devices, the energy deposition spectra had clearly distinguishable peaks and were comparable to other

\*Corresponding author. Department of Physics and Astronomy, University of Nebraska, Lincoln, Lincoln, NE 68588-0111, USA. Tel.: +1 402 472 2709.

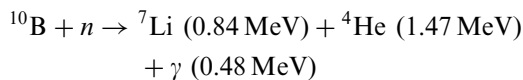
E-mail addresses: [clundst@unlserve.unl.edu](mailto:clundst@unlserve.unl.edu) (C. Lundstedt), [sadenwal@unlserve.unl.edu](mailto:sadenwal@unlserve.unl.edu) (S. Adenwalla).

devices based on boron [19]. This detector was fabricated with unenriched boron; the fraction of  $^{10}\text{B}$  in naturally occurring boron is close to 20%.

Previous calculations [20] indicate low energy tailing in the case of conversion layer detectors. The case of a heterojunction diode has not been addressed in [20], unlike the present work a complete Monte Carlo simulation for neutron capture, subsequent emission of ion pairs and their resulting trajectories and energy loss was not used. Rather a simplified Monte Carlo procedure to calculate the energy deposition of the ions was used. In this paper, we calculate, both analytically with a simplified physical model and by using the well-characterized, mature Monte Carlo detector simulation program *GEANT* (*GEometry ANd Tracking*) [21,22] the energy deposition spectra for various BC based planar, non-sandwich devices. These results are important in order to establish criteria for distinguishing between conversion layer devices and true diodes. These techniques are also important for assessing the ultimate efficiency of these and other solid state neutron detectors.

## 1. Detector phenomenology

The basic reactions for slow neutron capture by  $^{10}\text{B}$  are well known. The  $^{10}\text{B}$  nucleus absorbs the neutron and then promptly decays via one of two decay channels:



The branching fractions of these decays when the incident neutron is thermal are 94% and 6%, respectively, and the reactions yield the kinetic energies listed in parentheses. The kinetic energies were calculated using the capture energy release (Q-value) and atomic masses consistent with those found in Ref. [23].

Momentum conservation dictates that the lithium (Li) and helium ( $\alpha$ ) recoil in opposite directions if the captured neutron had zero kinetic energy. The range of each ion is a few  $\mu\text{m}$  in solid materials [23]. In our calculations, we vary the thickness of the BC layer, while keeping the thickness of Si sufficiently large to ensure ion capture.

In Fig. 1 we indicate the geometric constraints on the device(s). Neutron capture occurs at a depth  $z$  in the BC layer of thickness  $t$ , leading to the emission of two energetic charged particles, flying apart in opposite directions. In both instances shown, the Li particle enters the silicon, but the scenario in which the He ion enters the silicon is equally probable. The ions can begin at any angle with equal probability; in Fig. 1 we illustrate the paths of the ions that start with two particular angles, measured with respect to the normal to the film,  $\theta_1$  and  $\theta_2$ . The Li ion in path 1 deposits most of its energy into the Si, with a small fraction being deposited into the BC, whereas the corresponding He ion deposits a fractional amount of its energy into the BC.

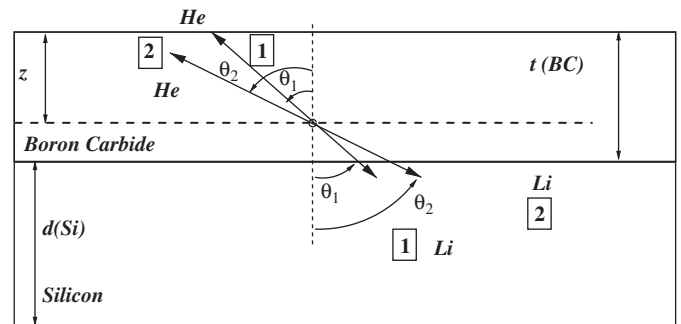


Fig. 1. Two typical neutron capture events in a planar non-sandwich detector. In this figure, neutron capture and the subsequent production of He and Li ions occur at a depth  $z$  in a boron carbide layer of thickness  $t$ . The figure depicts two scenarios, one in which only the Li ion is captured (path 1) and one in which both ions are captured (path 2, for further details see text).

If the BC were to act merely as a conversion layer, the contribution to the resulting energy deposition spectra for this configuration would occur only at the energy corresponding to the portion of Li ion energy that was deposited in the Si. This situation is effectively the same as a boron rich layer electrically external to a Schottky barrier silicon diode with a vanishingly thin barrier metal layer [7]. If, however, the BC is an active part of the device in which the acquisition of charge in the BC layer is similar to that in the silicon, the total contributing energy is the sum of the energy deposited by the He ion in the BC plus the total energy of the Li ion. The energy deposited by the He in the BC varies with angle,  $\theta_1$  and has a continuous range of values, leading to the higher energy tailing seen in Fig. 2.

Path 2 in Fig. 1 depicts a scenario in which both ions are stopped in the device. In the case of a conversion layer device, none of the energy deposited in the neutron capture layer leads to an electrical signal; hence the spectral energy contribution occurs at the fractional energy deposited into the Si by the Li ion. For a diode device with an active BC layer however, both parts of the device capture the charges, leading to a *full-energy* peak at the *sum* of the He and Li energies.

## 2. Monte Carlo simulation

The Monte Carlo simulation toolkit used for this analysis was *GEANT* version 4.5.2 [21]. The *GEANT* simulation software is often used with large scale, high energy particle experiments; however, a design overhaul of *GEANT* between versions 3 and 4 has created a generic toolkit that is appropriate to use at any energy regime. *GEANT4* is an object oriented, C++ toolkit designed to track the passage of particles through various materials.

*GEANT* handles the entire physical simulation including detector construction (materials and geometry), neutron transport, capture cross-sections, ion production and tracking, but the most important aspect of *GEANT* with regard to this study is its treatment of energy loss of ions

through a material.<sup>1</sup> The fractional amount of energy lost by each ion during its traverse of the relevant part(s) of the device is used for constructing the energy deposition spectra.

For charged particles as heavy as the helium (He) and lithium (Li) created in the neutron capture process, GEANT uses an energy dependent technique based on data. The techniques for calculating energy loss for ions are discussed in detail elsewhere [25,26]. Efforts are made here to explain the relevant algorithms used for He and Li energy loss.

### 2.1. Energy loss of $\alpha$ particles and lithium ions

The primary process for an ion to lose energy as it passes through a material is via interactions with the electrons within the material. At high energies,  $\sim 10$  MeV, this can be modeled using the Bethe–Bloch formula [27]. For the kinetic energies ( $E$ ) at which  $\alpha$  particles are created in the neutron capture by boron,  $E < 2$  MeV, GEANT uses the Ziegler parameterization [28]

$$S_e = \frac{S_{\text{low}} S_{\text{high}}}{S_{\text{low}} + S_{\text{high}}},$$

$$S_{\text{low}} = A_1 E^{A_2},$$

$$S_{\text{high}} = \frac{A_3}{E} \ln \left( 1 + \frac{A_4}{E} + A_5 E \right) \quad (1)$$

where  $S_e$  is given as the electronic stopping power in units of [eV/10<sup>15</sup> atoms/cm<sup>2</sup>] and the  $A_j$  parameters are fit from atom-specific data provided by the International Commission on Radiation Units and Measurement (ICRU), [29].

To calculate the energy loss of the ion as it passes through a compound GEANT treats the compound as a continuum of pure elements proportionally weighted to the electron density of the element in the absorber. In this treatment, the electronic stopping power of the compound is expressed as the sum of the stopping powers of the individual elements:

$$S_e = \sum_j S_{ej}. \quad (2)$$

Our GEANT simulation makes the following assumptions:

- The energy deposited by the Li and He ions in the material is ALL converted into electron hole pairs.
- All charges generated are collected by the electrodes i.e. there is no recombination. The depletion region extends through the thickness of both BC and Si traversed by the ions.
- The ions are not scattered by the underlying lattice (a reasonable assumption at MeV energies).
- The simulated boron is 19% <sup>10</sup>B and 81% <sup>11</sup>B (unenriched) for consistency with fabricated devices.

- There is no electronic noise or other process that affects the detected energies in pulse height spectra. We do consider electronic noise and the subsequent smearing of the pulse height spectrum in Section 4.

Furthermore, 10<sup>7</sup> neutrons were simulated at normal incidence for each detector geometry. However, all simulation output has been normalized to show the relative intensity per incident neutron to allow for easy comparison to the analytical techniques.

The GEANT simulator also creates the lithium and  $\alpha$  decay products with slightly different kinetic energy than is generally found in the literature or calculated using conservation of energy. GEANT gives the energies of the Li to be 830 keV and 1.0 MeV for the two decay processes and the alpha energies at 1.45 and 1.77 MeV. These energies are slightly different from the capture product energies in Ref. [23] already given in Section 1. The calculations that determine these particle energies are internal to the GEANT toolkit and were not adjusted for this simulation.

### 3. Simple physical model

Described here is a physical model that captures the main features of energy deposition relevant to neutron capture and capture product energy deposition in both conversion-layer and electrically-active-capture-layer devices that are based on boron. We simulated the energy spectra on the basis of continuous slowing down of ions traveling along straight paths since, to a first approximation, a light ion losses energy at a constant rate along its path in a material and the paths of energetic light ions are relatively straight until their energies become quite low.

This calculation of the energy spectra of the  $\alpha$  and Li ion products of neutron capture by boron-10 (<sup>10</sup>B) is for the case of neutrons incident normal to the neutron-capture layer. Each spectrum calculation is carried out separately for both initial energies of both capture products. The spectra are calculated for the energy deposited within the <sup>10</sup>B containing layer as well as escaping through the neutron entrance and exit surfaces of the <sup>10</sup>B containing layer. For simplicity, the thickness of the capture layer is taken to be small enough compared with the path length for neutron capture that the probability density of capture of each neutron can be considered constant through the thickness of the capture layer. This enables the conversion layer and heterojunction diode spectra to be calculated analytically.

#### 3.1. Approximations

The simulation relies on the following approximations:

- Only the capture reaction ions are simulated and the gamma ray is ignored. This is entirely justified since the gamma ray energy is 0.48 MeV and the linear absorption coefficient for such gammas in BC is very small (since the atomic numbers of boron and carbon are so low).

<sup>1</sup>GEANT contains a large number of physics processes that can be switched on and off in the simulation. The physics processes included in our simulation are listed in [24].

- Constant slowing down is assumed along the path of each capture product within the B-containing layer. This means that the change in energy deposition rate described by Eq. (1) is omitted.
- Capture products are taken to follow straight paths until they stop or escape from the  $^{10}\text{B}$  containing layer. Thus the calculation ignores the angular scattering of ions at any point along their paths.
- Capture products start in exactly opposite directions. Thus, the calculation ignores the influence of any initial neutron kinetic energy on the emission of reaction products. This is the case for thermal and cold neutrons.
- Capture products are assumed to be emitted in the ratio, and with the energies, given in the capture reactions above. This is fully justified for the capture of thermal and cold neutrons.
- Capture products that leave the layer do not return to the layer.
- The layer is parallel-sided and infinitely wide compared with its thickness.

### 3.2. Calculation

We seek two measures of performance: (1) the total probability  $N$  that an incident thermal neutron will result in a potentially detectable capture ion outcome—in essence the potential thermal neutron detection efficiency assuming perfect collection of the ions which have non-zero kinetic energies—and (2) the probability distribution  $dN/dE$  that an incident thermal neutron will result in a potentially detectable ion outcome in the energy range  $dE$  about each energy  $E$ —effectively the energy spectrum of thermal neutron capture outcomes assuming perfect collection of the charge generated by the ion in each case.

For simplicity, we assume that an incident thermal neutron can be captured with constant probability,  $n$ , per unit depth into the neutron capture layer. This introduces minimal error in the case of thermal and epithermal energy neutrons whose neutron capture mean free paths greatly exceed the thickness of the capture layer. In the case of normal incidence,  $n$  is the inverse of the length commonly known as the macroscopic neutron capture cross-section—the product of the capture cross-section per atom and the number density of the capture atoms.

Consider the case of a neutron capture at a depth  $z$  into the layer resulting in capture reaction product ions traveling in opposite directions at an angle  $\theta$  with respect to the normal to the capture layer. The energy “lost”, meaning “deposited”, by an ion during its escape from depth  $z$  in a direction  $\theta$  is:

$$E_L = \frac{Sz}{\cos\theta} \quad (3)$$

where the stopping power of the ion in the layer is  $S = E_{\text{ion}}/R$ , with  $E_{\text{ion}}$  and  $R$  being the initial energy and

the total range of this capture ion in the layer. We use the expression “energy lost” to emphasize that for the conversion layer case this energy is in fact unavailable for detection. Use of this ‘lost energy’ is however the key to the major gain in performance that is potentially accessible with an all BC device and with other devices which make use of the semiconducting character of the neutron capture layer.

Since  $E_{\text{ion}}$  and  $R$  differ for each of the capture products and also depend on whether a gamma is emitted in the capture reaction, calculations must be performed separately for each capture product ion type—four calculations therefore. Each calculation for a capture product ion also requires the subsequent calculation of its companion ion since each capture results in production of ion pairs. The calculations for the companion ion proceed in the same manner shown here, but since the ion is headed in the opposite direction, the capture depth,  $z$ , value is replaced with the remaining film thickness behind the capture depth,  $(t - z)$ .

At any capture location in the layer, capture product ion pairs have equal probability of originating in any direction. The fraction of pairs,  $d\eta$ , emitted in the range  $\theta - \theta + d\theta$  is equal to the fraction  $d\Omega/4\pi$  of all solid angles contained in that angle range and can be represented as

$$d\eta = \frac{d\Omega}{4\pi} = \frac{2\pi \sin\theta d\theta}{4\pi} = -\frac{1}{2}d(\cos\theta). \quad (4)$$

In order to obtain an expression for the energy distributions of capture ions originating at depth  $z$ , we note that Eq. (3) couples  $\cos\theta$  and energy loss  $E_L$  for a capture ion originating from depth  $z$  in the capture layer. Therefore, to evaluate the probability  $d\eta/dE_L|_z$  that a particular capture product ion could escape from depth  $z$  after losing energy in the range  $dE_L$  about  $E_L$ , we write

$$\left. \frac{d\eta}{dE_L} \right|_z = \left. \frac{d\eta}{d(\cos\theta)} \cdot \frac{d(\cos\theta)}{dE_L} \right|_z. \quad (5)$$

Using Eqs. (3), (4) in Eq. (5), we obtain

$$\left. \frac{d\eta}{dE_L} \right|_z = \left. \frac{Sz}{2E_L^2} \right|_z. \quad (6)$$

To calculate the probability that an incident neutron could result in capture product ion escape from depths in the range  $dz$  about  $z$  after losing energy in the range  $dE_L$  about  $E_L$ , both sides of Eq. (6) must be multiplied by  $ndz$ , the probability that a neutron will be captured in the depth range  $dz$ :

$$(ndz) \left. \frac{d\eta}{dE_L} \right|_z = (ndz) \left. \frac{Sz}{2E_L^2} \right|_z. \quad (7)$$

The probability that an incident neutron will be captured in a layer of thickness  $t$  and will result in escape of a capture product ion which has lost energy in the range  $dE_L$  about  $E_L$  is

$$\left. \frac{dN}{dE_L} \right|_z = \int_0^t n \left. \frac{d\eta}{dE_L} \right|_z dz. \quad (8)$$

Substituting Eq. (7) into Eq. (8) and taking into account that  $z$  may not exceed  $t$ , we obtain the neutron capture ion escape probability energy loss distribution:

$$\frac{dN}{dE_L} = \begin{cases} \frac{n}{4S} & \text{for } E_L \leq St, \\ \frac{nSt^2}{4E_L^2} & \text{for } E_L > St. \end{cases} \quad (9)$$

Since  $E_L \leq E_{\text{ion}}$  by definition, capture ions cannot escape from depths exceeding  $E_{\text{ion}}/S$ . So, if layer thickness  $t$  exceeds  $E_{\text{ion}}/S$ , capture ions cannot escape from part of the capture layer and for these ions Eq. (9) reduces to

$$\frac{dN}{dE_L} = \frac{n}{4S} \quad \text{for } E_L \leq E_{\text{ion}}. \quad (10)$$

### 3.3. Boron carbide conversion layer detector

In the conversion layer case, the maximum detectable energy of a capture product ion of original energy  $E_{\text{ion}}$  is the energy,  $E_r$ , that the ion retains on leaving the capture layer and entering an adjacent detector layer. This energy is determined simply by subtracting the energy lost in the capture layer,  $E_L$ , from the initial ion energy,  $E_{\text{ion}}$

$$E_r = E_{\text{ion}} - E_L. \quad (11)$$

The component spectrum for this original ion energy is then computed by placing  $dN/dE_L$ , the probability of a neutron capture resulting in an energy loss  $E_L$  calculated using Eq. (9), or Eq. (10) if appropriate, in the energy channel corresponding to  $E_r$ . By repeating this for each  $E_L$  up to  $E_{\text{ion}}$ , the full capture ion product spectrum can be evaluated. The summation of all four component spectra yields the total probability spectra seen in the conversion layer parts of Figs. 2–4.

### 3.4. Heterojunction diode detector

The case corresponding to a diode junction formed by neutron capturing boron carbide semiconductor and another semiconductor may be evaluated analytically much as for the conversion layer. We make two extra assumptions for the heterojunction diode case: (1) the capture layer and the adjacent semiconductor that form the diode are suitably matched for electrical properties, and (2) the depletion region extends through the thickness of the boron carbide layer and extends at least as far as the maximum ion range in the other semiconductor. In this case, the only capture ion pair product energy that is not deposited in the heterojunction diode will be the energy,  $E_r$ , retained by an ion if it escapes through the surface of the capture layer opposite to the other semiconductor. As shown in Eq. (11), this energy is determined simply by subtracting the energy lost in the capture layer,  $E_L$ , from the initial ion energy,  $E_{\text{ion}}$ . Subtraction of  $E_r$  from the full initial energy,  $E_{\text{full}}$ , of the ion pair,  $E_{\text{ion1}} + E_{\text{ion2}}$ , yields the

total capture product ion energy deposited,  $E_T$ , in the diode per neutron capture:

$$\begin{aligned} E_T &= E_{\text{full}} - E_r \\ &= (E_{\text{ion1}} + E_{\text{ion2}}) - (E_{\text{ion1}} - E_L) \\ &= E_{\text{ion2}} + E_L. \end{aligned} \quad (12)$$

Here ion1 is the ion which could escape from the diode without depositing all its energy and ion2 remains in the diode and deposits all its energy there.

The component spectra in this case are then formed by placing the above probability,  $dN/dE_L$ , that an ion (labeled ion1 in Eq. (12)) has lost energy  $E_L$  before leaving the capture layer, in the energy channel containing  $E_T$ , the energy deposited in the capture layer and adjacent semiconductor. Note that if ion1 does not escape the capture layer, then  $E_T = E_{\text{full}}$ . To ensure correct counting of captures, the probability that capture results in deposition of energy  $E_{\text{full}}$  is obtained by subtracting the integral of all component spectra at energies other than  $E_{\text{full}}$  from the total probability of capture in the layer. The summations of the component spectra again yield the total heterojunction diode probability spectra shown in Figs. 2–4.

### 3.5. All boron carbide neutron detector

To model the case of a solid state neutron detector in which the only semiconductor is the BC capture layer, i.e. the all BC neutron detector, calculation proceeds in a similar manner to the heterojunction diode case, but the total ion energy,  $E_T$ , deposited as a result of a neutron capture becomes:

$$\begin{aligned} E_T &= E_{\text{full}} - E_{r1} - E_{r2} \\ &= (E_{\text{ion1}} + E_{\text{ion2}}) - (E_{\text{ion1}} - E_{L1}) - (E_{\text{ion2}} - E_{L2}) \\ &= E_{L1} + E_{L2}. \end{aligned} \quad (13)$$

Here  $E_{r1}$  and  $E_{r2}$  are the energies retained by the two ions of a single capture pair if they escape the capture layer and are set, respectively, to zero if either does not escape. Note that the total energy detectable is the “energy lost” by the ion pair as discussed before. Although the energy deposited in the layer by each ion is simply evaluated from Eq. (3) for each capture depth  $z$ , or  $t - z$  as needed, and for each capture ion starting angle  $\theta$ , the construction of the all BC detector capture ion deposition spectrum requires numerical evaluation. This difference in calculation is required since both ions deposit energy in the layer and each of the ions in a capture product ion pair present differing stopping powers,  $S$ , resulting in different energy losses,  $E_L$ . Therefore the evaluation of the all BC ion energy deposition spectrum depends on summing over all neutron capture locations and all the initial angles of the capture ion pairs. For each  $z$  and  $\cos\theta$ ,  $E_L$  for each capture ion is calculated using Eq. (3). These  $E_L$  values are then used to determine  $E_T$  using Eq. (13). The total probability spectrum for the all BC device is obtained by stepping

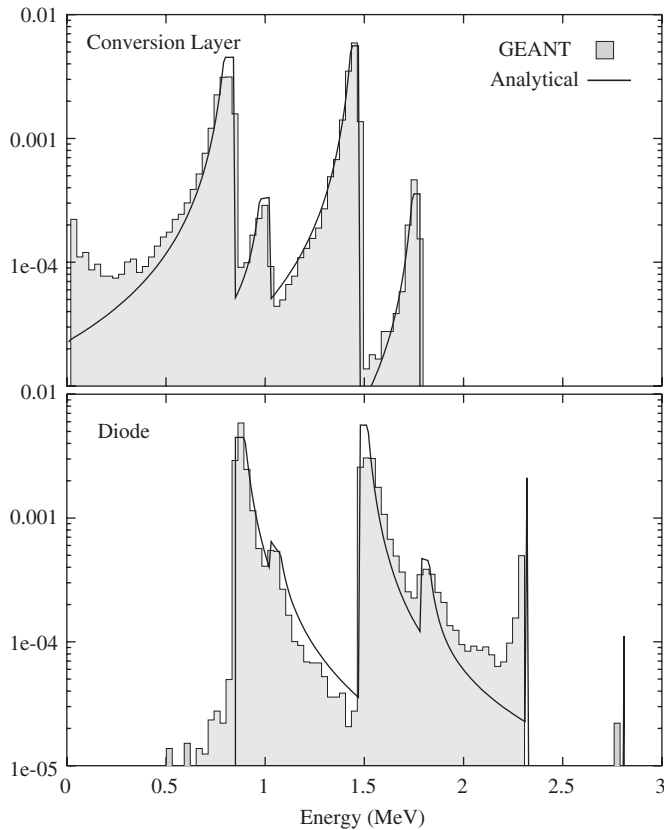


Fig. 2. Energy deposition spectra for boron carbide neutron detectors calculated using *GEANT* and the simplified physical model. The boron carbide layer thickness is 100 nm and a silicon layer thickness of 5 cm (much larger than the thickness of the depletion region). The upper (lower) panel corresponds to a conversion (heterojunction diode) detector. The gray region in the plot shows the spectrum calculated using *GEANT*. The y-axis shows the counts per incident neutron.

through the layer thickness, evaluating the energy  $E_T$  for each depth and angle combination, and adding the appropriate probability increment to the energy channel corresponding to  $E_T$ . This probability increment  $P_{z,\theta}$ , is just the total probability of neutron capture in the capture layer divided by the number of depth and angle combinations:

$$P_{z,\theta} = \frac{nt}{1/\Delta(\cos\theta) * t/\Delta z} \quad (14)$$

where  $nt$  is the total number of captures in the layer and is divided by the total number of  $z$  and solid angle  $\cos\theta$  combinations. Adequately fine sampling was obtained by stepping through capture depth  $z$  in increments of  $\Delta z = 1$  nm and through emission function  $\cos\theta$  (in Eq. (4)), in steps of  $\Delta(\cos\theta) = 0.0005$ . For convenience, this evaluation was performed using MathCad [30]. Resultant probability spectra are given in Fig. 5.

#### 4. Results and discussions

Fig. 2 shows the energy deposition spectra for a 100 nm BC layer on Si. The upper panel shows a conversion layer

device, in which the BC captures the neutron and produces energetic ions, which then subsequently produce electron hole pairs in the semiconducting Si. The lower panel shows the neutron detection signature of a true diode detector, in which both neutron capture and charge creation occur in the BC layer, as well as charge capture in the Si layer. Immediately, one notices two significant differences. The conversion layer signatures have tailing towards lower energies than the initial capture product energies, while the diode devices have tailing towards higher energies. Moreover the diode detector shows the presence of two additional (weak) peaks at approximately 2.3 and 2.8 MeV. These are *full-energy* peaks, at the energies,  $E_{full}$ , of the sums of the Li and He ion energies that occur when both ions deposit all their energy in the device. This cannot occur in the conversion layer device, since charge is captured only in the Si layer and not in the conversion layer. Therefore, for instance, if the He ion deposits all its energy in the Si layer, the concurrent Li ion flies out (at  $180^\circ$ ) into the BC layer where no charge capture can occur. However, if the device is a diode instead, there is a small probability (constrained by geometric effects) that a particular He–Li pair can deposit all its energy in the device and produce the largest possible number of electron-hole pairs. The tailing effect can be similarly understood. If charge capture occurs only in the Si layer, whereas neutron capture occurs in the BC layer, most He and Li ions will deposit some energy in the BC layer before entering the Si layer (the exceptions are those that are captured right at the BC/Si interface). Hence these ions generate lower charge in the Si layer. In the diode detector, for every He ion that deposits all its energy in the Si, there is a Li ion that will generate some charge in the BC layer, leading to high energy tailing.

Figs. 3, 4 are similar plots for increasing thicknesses of BC. As the thickness of the BC layer increases, the peaks due to the individual He and Li ions become less distinct, and in the case of a diode detector, the *full-energy* peaks are most prominent. In the case of conversion layer devices, neutron capture further away from the BC/Si interface can occur, leading to even less of the ion energy being deposited in the Si, implying increased lower energy tailing. In the case of diode devices, the increased thickness allows for larger fractional energies being deposited into the BC, leading to increased high energy tailing. In both cases, a larger fraction of events deposit energy away from the initial energy peak of the He and Li ions, leading to a broader, flatter energy deposition spectra. In the case of diode devices, increasing the BC thickness increases the probability of capturing both reaction products and increases the height of the *full-energy* peaks.

Fig. 5 shows the energy deposition spectra produced by an all BC device, for example a homojunction diode [16]. Each of the spectra rises rapidly at energies above the minimum corresponding to the energy deposition by the He ion traversing the minimum length path through the full thickness of the BC material (i.e. the path corresponding to

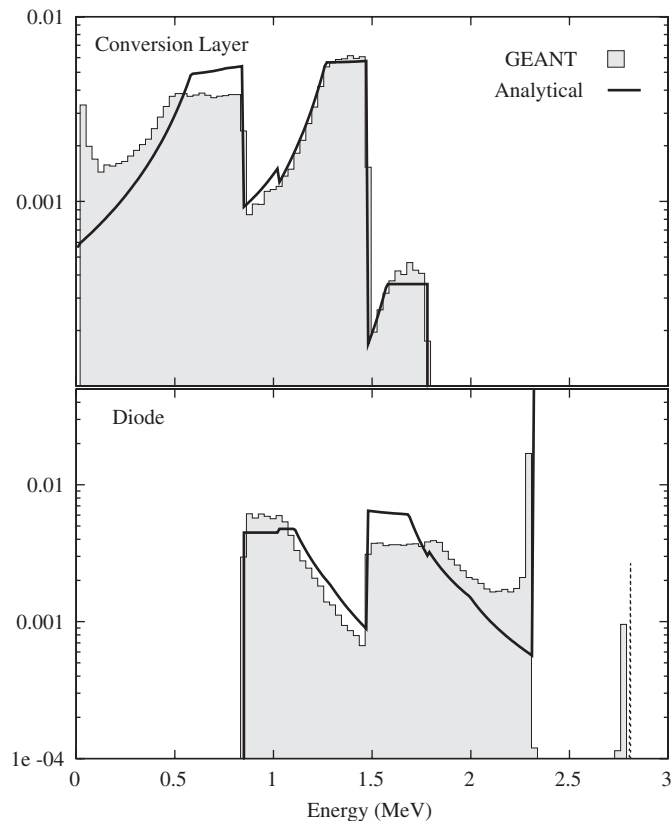


Fig. 3. Energy deposition spectra for boron carbide neutron detectors calculated using GEANT and the simplified physical model. The boron carbide layer thickness is 500 nm and a silicon layer thickness of 5 cm. The upper (lower) panel corresponds to a conversion (heterojunction diode) detector. The gray region in the plot shows the spectrum calculated using GEANT. The y-axis shows the counts per incident neutron.

$\theta = 0$ ). Corresponding to the equivalent minimum energy that is allowed for Li ion energy deposition, there is a continuing increase at somewhat higher energies, since the stopping power for the Li ion is roughly twice that for the He ion. For thicknesses in the range up to 1000 nm, the minimum energy found in the spectra therefore scales exactly in proportion to the thickness. For a thickness of 100 nm, well below the path length of the ions, the spectra have weak *full-energy* peaks since so few ions are geometrically likely to deposit anything approaching their full energies in such a thin device. With increasing thickness, the range of angles of capture product ions that result in longer paths in the BC increases and so the high-energy content of the spectra also increases. The peaks corresponding to full energy deposition by both capture product ions scale with thickness. These spectra are similar to those seen in  $\text{BF}_3$  gas counters [5,6].

We have given some examples of the ideal spectra for both conversion and semiconducting classes of BC-containing detectors with the natural abundance boron and capture layers that are substantially thinner than the shortest range of the  $^{10}\text{B}$  capture products. For detectors relying on charge collection within thin semi-

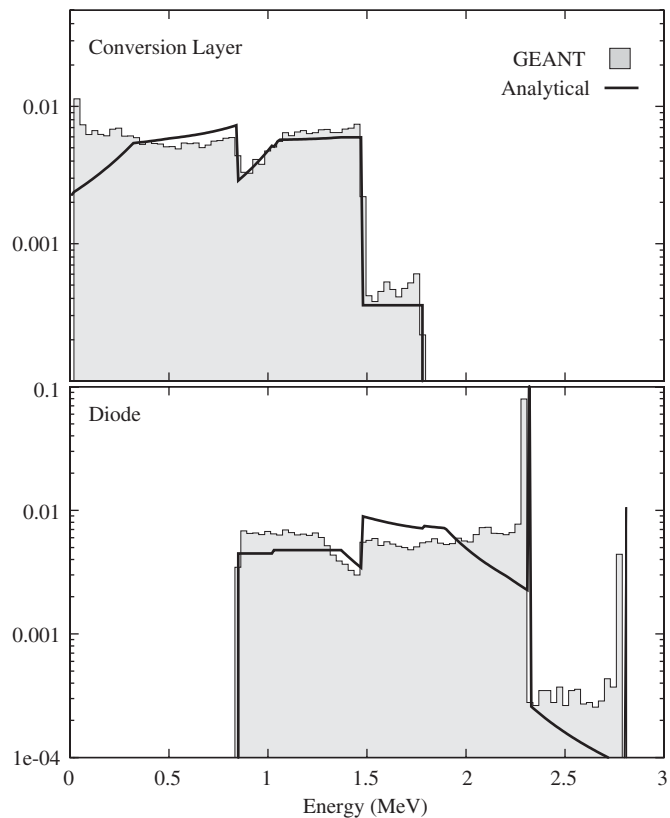


Fig. 4. Energy deposition spectra for boron carbide neutron detectors calculated using GEANT and the simplified physical model. The boron carbide layer thickness is 1000 nm and a silicon layer thickness of 5 cm. The upper (lower) panel corresponds to a conversion (heterojunction diode) detector. The gray region in the plot shows the spectrum calculated using GEANT. The y-axis shows the counts per incident neutron.

conducting BC, the relative contributions of the spectral products are strongly dependent on thickness. Using a simple solid angle calculation the fraction of neutron captures that contribute to a sum peak are 0.025, 0.125 and 0.25 for 100, 500 and 1000 nm BC, respectively, in a heterojunction diode.

The spectra shown in Figs. 2–4 do not contain electronic measurement effects which could significantly diminish the prominence, for example, of the full-energy peaks. To demonstrate measurement effects somewhat realistically, we measured the noise peak of the detector electronics system we use at the University of Nebraska. The measured noise peak was well fitted by a Gaussian peak with 32 keV full-width at half maximum. The results of smearing the GEANT simulation of the 500 nm BC devices is shown in Fig. 6. A full-energy peak height reduction by a factor of five is observed in the diode case but with little other major change in the spectral shape.

## 5. Conclusions

This paper provides a simulation of energy deposition spectra for solid-state neutron detectors, using both a

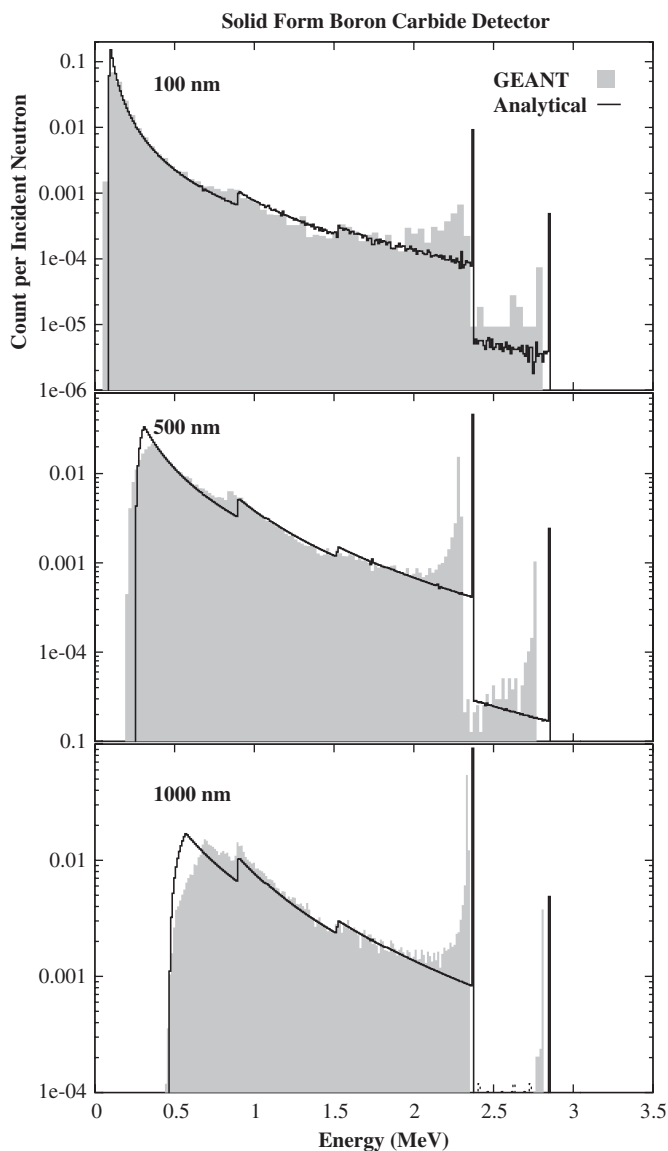


Fig. 5. Energy deposition spectra for boron carbide neutron detectors calculated using GEANT and the simplified physical model. Each panel corresponds to a solid form boron carbide detector of a given thickness. The top panel shows 100 nm thickness, the middle panel shows 500 nm thickness and the bottom panel shows a 1000 nm thick detector.

Monte Carlo simulation and a simple physical model. The generally good agreement between the simple physical model and the GEANT simulations make it clear that the simple physical model can provide not only a good quantitative basis for evaluating the efficiencies of the various detector types as a function of capture layer thickness but also quantitatively useful estimates of the ion-deposited energy spectra for each of the detector types. The differences correspond largely to the changes in direction and rate of energy deposition of the ions when they have little residual kinetic energy. It is straightforward to extend the simplified physical model to capture layers that are no longer thin compared with the neutron absorption length; this requires numerical evaluation of the results just as in the case of evaluating spectra that

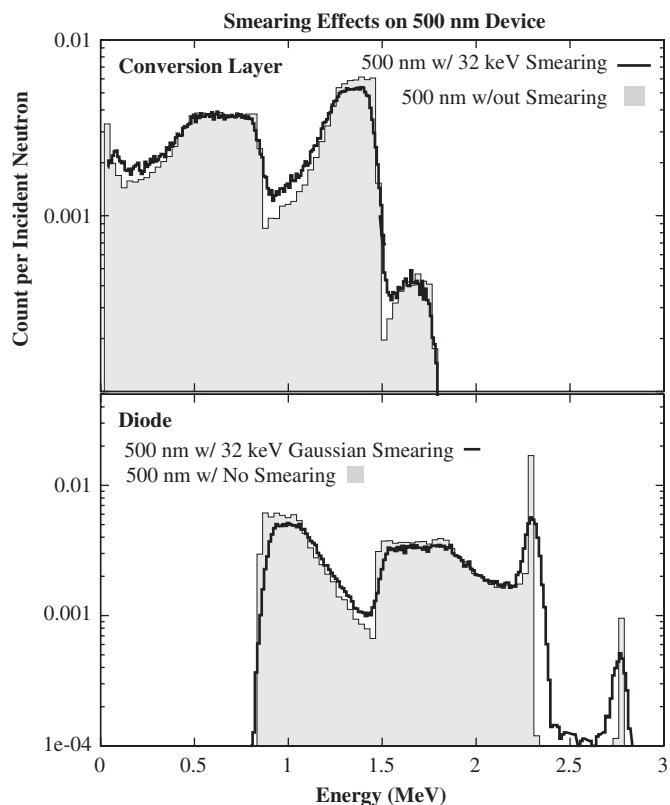


Fig. 6. Energy deposition spectra for boron carbide neutron detectors calculated using GEANT. The boron carbide layer thickness is 500 nm and a silicon layer thickness of 5 cm. The results were scaled for intensity per incident neutron. The upper (lower) panel corresponds to a conversion (heterojunction diode) detector. The unfilled region in the plot shows the spectrum smeared with a 32 keV Gaussian noise peak.

involve partial energy deposition by both capture ions. The intuitive understanding afforded by the physical model allows for a quick and easy evaluation of experimentally obtained energy deposition spectra. Clearly, the assumptions and approximations made in both the GEANT and simplified approaches presented in this paper lead to some idealizations in the final results. Specifically, the electron-hole pair generation statistics and the electronic device and amplifier noise, as well as any recombination of charges and charge trapping, will lead to broadening of features in the energy deposition spectra and may cause variations on the spectral shapes presented here.

We conclude that both GEANT and the simplified physical model provide experimentally verifiable criteria for distinguishing between conversion layer neutron detectors and detectors based on semiconducting neutron capture material in the case of ideal charge collection and handling in both detector classes. Conversion layer detector spectra have tailing only on the low energy side of each of the initial capture product energies and have no peaks corresponding to complete collection of capture product He and Li pairs (*full-energy* peaks). Semiconducting capture material detectors exhibit tailing on the high energy side of each of these initial capture product energies and exhibit *full-energy* peaks. In reality, the differences

may not be so clear-cut and there may be changes in tailing or changes in relative prominence of spectral features or mixing of conversion and semiconducting detector class spectral characteristics. These changes can occur because real detectors, of course, do not have ideal charge collection and because charge pulse processing time behavior may not simultaneously be matched to the timing of charge availability from each charge generation region of the real detector. This latter matching is essential if the charge from all regions of the detector is to contribute to the observed spectra.

### Acknowledgements

This work is partially funded by the State of Nebraska, NASA-ASTID NNGO15GM89G U.S. Department of Energy National Nuclear Security Administration Office of Nonproliferation Research and Engineering [NA-22] through Pacific Northwest National Laboratory and Office of Naval Research N00014-04-1-0605.

### References

- [1] R. Cooper, I. Anderson, C. Britton, K. Crawford, L. Crow, P. DeLurgio, C. Hoffmann, D. Hutchinson, R. Klann, I. Naday, G. Smith, A Program for Neutron Detector Research and Development, SNS Neutron Detector White Paper, ([http://www.sns.gov/documentation/Neutron\\_Detector\\_White\\_Paper\\_March\\_03.pdf](http://www.sns.gov/documentation/Neutron_Detector_White_Paper_March_03.pdf)).
- [2] W.C. Feldman, W.V. Boynton, R.L. Tokar, T.H. Prettyman, O. Gasnault, S.W. Squyres, R.C. Elphic, D.J. Lawrence, S.L. Lawson, S. Maurice, G.W. McKinney, K.R. Moore, R.C. Reedy, *Science* 297 (2002) 75.
- [3] I. Mtrofanov, D. Anfirnov, A. Kozyrev, M. Litvak, A. Sanin, V. Tret'yakov, A. Krylov, V. Shvetsov, W.V. Boynton, C. Shinohara, D. Hamara, R.S. Suanders, *Science* 297 (2002) 78.
- [4] MARIE—Martian Radiation Environment Experiment, (<http://marie.jsc.nasa.gov/>).
- [5] S. Sakamoto, A. Morioka, *Nucl. Instr. and Meth. A* 353 (1994) 160.
- [6] R.W. Kavanagh, R.G. Marcle, *Phys. Rev. C* 36 (1987) 1194.
- [7] D.S. McGregor, et al., *Nucl. Instr. and Meth. A* 466 (2001) 126.
- [8] D.S. McGregor, et al., *IEEE Trans. Nucl. Sci NS-47* (2000) 1364.
- [9] A. Rose, *Nucl. Instr. and Meth. A* 52 (1967) 166.
- [10] S. Lee, et al., *J. Appl. Phys.* 72 (10) (1992) 4925.
- [11] B.W. Robertson, Megjun Bai, J. Strinz-Colborn, P.A. Dowben, Boron-Carbon alloy development for use in high temperature devices and sensors, in: *Proceedings of Second European Conference on High Temperature Electronics (HITEN '97)*, AEA Technology, Didcot, UK, 1998, pp. 219–224.
- [12] S. Adenwalla, P. Welsch, A. Harken, J.I. Brand, A. Sezer, B.W. Robertson, *Appl. Phys. Lett.* 79 (2001) 4357.
- [13] S.D. Hwang, et al., *Appl. Phys. Lett.* 68 (11) (1996) 1495.
- [14] D. Byun, et al., *Nanostruct. Mater.* 5 (4) (1995) 465.
- [15] D. Byun, et al., *Appl. Phys. Lett.* 64 (15) (1994) 1968.
- [16] S.-D. Hwang, et al., *Appl. Phys. Lett.* 72 (8) (1997) 1028.
- [17] B.W. Robertson, et al., *Appl. Phys. Lett.* 80 (19) (2002) 3644.
- [18] B.W. Robertson, S. Adenwalla, A. Harken, P. Welsch, J.I. Brand, J.P. Claassen, N.M. Boag, P.A. Dowben, Semiconducting boron-rich neutron detectors, in: I.S. Anderson, B. Guard (Eds.), *Advances in: Neutron Scattering Instrumentation*, Proc. SPIE, vol. 4785, 2002, pp. 226–233.
- [19] A. Harken, E. Day, B.W. Robertson, S. Adenwalla, *JJAP* 44 (1A) (2005) 444.
- [20] D. McGregor, et al., *Nucl. Instr. and Meth. A* 517 (2004) 180.
- [21] Geant4—A Simulation Toolkit, *Nucl. Instr. and Meth. A* 506 (2003) 250.
- [22] S. Giani, et al., GEANT4: An object-oriented toolkit for simulation in HEP, CERN/LHCC 98-44, (1998); GEANT4 Web page: (<http://cern.ch/geant4>).
- [23] G.F. Knoll, *Radiation Detection and Measurements*, Second ed., Wiley, New York, 1989.
- [24] GEANT Physics Processes by particle, Neutron Processes: Elastic Scattering, Low Energy Inelastic Scattering, Low Energy Fission, Low Energy Capture. Electrons/Positrons: Multiple Scattering, Ionisation, Bremsstrahlung. All other charged particles (ions): Multiple Scattering, Low Energy Ionisation, Low Energy Loss.
- [25] Giani, et al., GEANT4 Simulation of Energy Losses of Ions, CERN-99-300, INFN/AE-99/21, November, 1999.
- [26] V.N. Ivanchenko, et al., GEANT4 Simulation of Energy Losses of Slow Hadrons, CERN-99-121, INFN/AE-99/20, September, 1999.
- [27] C. Caso, et al. (Particle Data Group), *Eur. Phys. J. C* 3 (1998) 1.
- [28] J.F. Ziegler, *The Stopping and Ranges of Ions in Matter*, vol. 4, Pergamon Press, Oxford, 1977.
- [29] A. Allisey et al., ICRU Stopping Power and Ranges for Protons and  $\alpha$  Particles, ICRU Report 49, 1993.
- [30] *Mathcad 2000 User's Guide*, Second Printing, November, 1999.